Construction and Building Materials 173 (2018) 672–686

Contents lists available at ScienceDirect

Construction and Building Materials

journal homepage: www.elsevier.com/locate/conbuildmat

Experimental and numerical investigations on seismic responses of reinforced concrete structures considering strain rate effect

Hao Zhang [a], Hong-Nan Li [a,b], Chao Li [b,*], Guang-Wei Cao [a]

[a] School of Civil Engineering, Shenyang Jianzhu University, Shenyang 110168, Liaoning, China
[b] Faculty of Infrastructure Engineering, Dalian University of Technology, Dalian 116024, Liaoning, China

HIGHLIGHTS

- DIFs for the key material parameters of micro-concrete and iron wire are suggested.
- Shaking table test of a 1/5 scaled RC structural model is conducted.
- A three-dimensional rate-dependent fiber beam-column element model is proposed.
- Effectiveness of the proposed model is validated by the shaking table test data.

ARTICLE INFO

Article history:
Received 26 January 2018
Received in revised form 8 April 2018
Accepted 10 April 2018

Keywords:
RC structures
Strain rate effect
Shaking table test
Fiber beam-column element
Seismic response

ABSTRACT

The strain rate effect can inevitably impact the seismic responses of reinforced concrete (RC) structures because the dynamic properties of RC materials under earthquakes change significantly with the time-varying loading rates. This paper carries out systematic experimental tests and numerical simulations to investigate the effects of strain rates on the seismic responses of RC structures. The dynamic properties of micro-concrete and iron wire used in the shaking table specimen are firstly tested under seismic loading rates and the corresponding dynamic increase factors (DIFs) are estimated based on the test data. The shaking table test of a 1/5 scaled RC structure is performed to realistically reproduce the dynamic responses of RC structures with strain rate effect. Moreover, a three-dimensional rate-dependent fiber beam-column element is developed in the ABAQUS platform to establish the finite element (FE) model of the shaking table specimen, in which the estimated DIFs for the key parameters of micro-concrete and iron wire are employed to consider the strain rate effect. Besides, the rate-independent structural FE model is also developed using the traditional beam-column element with the static RC material constitutive models. The numerical results demonstrate that the seismic responses of RC structures are overestimated when the strain rate effect is neglected. As validated by the experimental data of the shaking table test, the FE model developed using the proposed rate-dependent fiber beam-column element can yield better structural seismic response predictions in comparison with the rate-independent model.

1. Introduction

Reinforced concrete (RC) structures have been extensively used in multistory and high-rise buildings due to their advantages of excellent structural integrity, durability and high economic efficiency. During their service periods, RC structures may be subjected to strong earthquake ground motions. The strain rates of reinforcing steel and concrete materials at critical sections of RC structural members may reach as high as 1 s^{-1}. Fu et al. [1] and Bischoff and Perry [2] systematically reviewed the compressive behavior of concrete at high strain rates, while the strain rate effect on the tensile strength of concrete was reviewed by Malvar and Rose [3] and Thomas and Sorensen [4]. It was reported that the compressive and tensile strength of concrete can be obviously increased at the strain rates induced by seismic loading. Moreover, the tensile strength of concrete is more susceptible to increase than the compressive strength. In addition, the mechanical properties of reinforcing steels under seismic strain rates were also examined by many researchers through dynamic loading tests [5–12]. The experimental findings indicated that the yield strength and ultimate tensile strength of reinforcing steels increase linearly with the logarithmical increase of strain rate, and the effect of strain rate

* Corresponding author.
E-mail address: chao.li@mail.dlut.edu.cn (C. Li).

https://doi.org/10.1016/j.conbuildmat.2018.04.085
0950-0618/

on the lower strength reinforcing steels is more significant as compared with that on the higher strength reinforcing steels.

In current literature, many investigations are focused on the effects of loading rates on the seismic behavior of RC members. The dynamic tests of simply supported and doubly reinforced beams were performed by Bertero et al. [13] to assess the influence of loading rate on the behavior of RC beams. It was found that the stiffness before the first yielding of reinforcing steel for the beams under the higher loading rate increases about 10% as compared with that for the beams under the lower loading rate. Significantly increases in the initial yield strength were also observed, but the effect of loading rate on the ultimate strength, flexural failure mode, measured strain, curvature and deflection ductility factors of the beams is not evident. The similar conclusions were obtained by Kulkarni and Shah [14], who carried out the experimental tests of seven pairs of RC beams subjected to static and high loading rates. It was also reported in the aforementioned studies that the failure mode of the RC beams may shift from brittle shear failure at the lower strain rate to the ductile flexural failure at higher strain rates. Otani et al. [15] performed a series of tests on four pairs of cantilever RC beams under static and dynamic loads to study the potential effects of strain rate. The specimens were tested in the vertical position and loaded horizontally using a dynamic actuator. The results showed that the seismic strain rate increased the flexural resistance of RC beams by 7%–20%. Li and Li [16] studied the dynamic behavior of simply supported RC beams with different shear spans through dynamic tests, in which the influence of loading rate on the bearing capacity, ductility, stiffness, failure mode and energy absorbing of beam specimens were systematically analyzed.

Ghannoum et al. [17] investigated the dynamic behaviors of RC columns subjected to the cyclic loadings at different strain rates. The test results showed that the lateral bearing capacity of RC columns can increase up to 33% when the loading rates are taken into account. The mechanical properties of RC columns under multi-dimensional dynamic loadings were investigated by Wang et al. [18]. Comparisons of test results indicated that the strength, stiffness, ductility, damage, energy absorption and failure mode were all influenced by the loading rate. Carrillo and Alcocer [19] studied the seismic performance of 12 RC walls using the quasi-static cyclic loading and shaking table tests. It was observed that stiffness and strength degradation properties of RC walls were dependent on the loading rate.

It should be noted that most of the previous studies are focused on the mechanical properties of RC materials or members under quasi-static and dynamic loadings through the laboratory tests. However, the experimental studies on the influence of strain rate on the seismic responses of RC structures are very rare. Numerical simulation method can provide an alternative way to effectively and practically predict the seismic responses of RC structures with inclusion of strain rate effect. Pandey et al. [20] analyzed the transient dynamic responses of three-dimensional RC structures based on a strain rate dependent concrete model. Guner and Vecchio [21] conducted the global seismic response analyses of RC frame structures, in which the strain rate effects are considered using the dynamic increase factors (DIFs) of concrete and reinforcing steel materials. Wang et al. [22] numerically studied the effect of strain rate on the seismic behaviors of recycled aggregate concrete frame structures. Moreover, the influence of strain rate on the seismic responses and fragilities of RC structures was examined by Asprone et al. [23]. The above-mentioned numerical investigations demonstrated that the rate-dependent properties of RC materials should be reasonably taken into consideration to precisely predict the seismic responses of RC frame structures.

Up to date, shaking table test is universally acknowledged to be the most appropriate and accurate method for reproducing the seismic dynamic responses of RC structures since the actual strain rate effects of RC materials under earthquake excitations can be experienced. In this paper, the shaking table test of a 1/5 scaled RC structure is performed to investigate the effects of strain rates on the dynamic responses of RC structures under earthquake excitations. The dynamic properties of micro-concrete and iron wire used in the test specimen are experimentally investigated under seismic loading rates and the corresponding DIFs are estimated based on the regression analyses of the test results. Moreover, a three-dimensional rate-dependent beam-column element model with fiber sections is developed for the numerical simulation of seismic responses of RC structures with inclusion of strain rate effect. The ABAQUS analysis platform is employed to develop the three-dimensional finite element (FE) model of the shaking table specimen, in which the estimated DIFs are used to simulate the rate-dependent properties of the micro-concrete and iron wire. The numerically calculated structural seismic responses are validated by the experimental data obtained from the shaking table test. The effects of strain rates on the seismic performance of the RC structure are analyzed and discussed in detail.

2. Dynamic loading tests of the materials in shaking table specimen

To fabricate scaled RC structural models for shaking table tests, the micro-concrete and iron wire are commonly used to replace the ordinary concrete and reinforcing steels in the prototype structure. In this section, the dynamic loading tests are conducted to investigate the rate-dependent properties of micro-concrete and iron wire used in the shaking table specimen. The DIFs for the key parameters of these two materials are estimated based on the regression analyses of the test results.

2.1. Micro-concrete

Micro-concrete is composed by a certain proportion of cement, silver sand, gravel (Diameter < 5 mm) and water, and its maximum compressive strength is generally less than 15 MPa. The quasi-static mechanical properties of micro-concrete were experimentally studied by Yang et al. [24]. It was revealed that stress-strain curves of micro-concrete are very similar to those of the ordinary concrete. Shen et al. [25] experimentally investigated the dynamic properties of micro-concrete under compression at different loading rates. The results illustrated that the dynamic compressive strength and elastic modulus of micro-concrete increase with strain rate, and the constitutive relation and failure mode are quite similar to those of ordinary concrete at different strain rates.

In this study, the uniaxial compressive tests of micro-concrete are conducted using the electro-hydraulic servo-controlled system under the loading rates of 10^{-5}–10^{-2} s^{-1}, which corresponds to the range of strain rates induced by seismic loading [2]. The dynamic test equipment and installation of micro-concrete specimen are shown in Fig. 1. The dimension of the micro-concrete cubic specimen is 100 mm × 100 mm × 100 mm, and the test specimens are cured simultaneously with the RC shaking table specimen in the natural environment. Table 1 presents the mixed proportions of the micro-concrete. The displacement control method was adopted in the test and the loading rate remains constant during each loading process. Moreover, the test data is recorded by a high speed data acquisition system. For each loading rate case, at least three specimens are tested and the number of specimens is increased if the dispersion of the test results is relatively large.

Based on the test results, the averaged stress-strain curves for the micro-concrete specimens at different strain rates are calculated, as plotted in Fig. 2. It can be observed that with the increase

(a) Test system (b) Specimen setup

Fig. 1. Dynamic test equipment and installation of micro-concrete specimens.

Table 1
Mixed proportion of micro-concrete in the test.

Cement	Fine sand	Gravel (D ≤ 5 mm)	Water
1	3.26	3.98	0.82

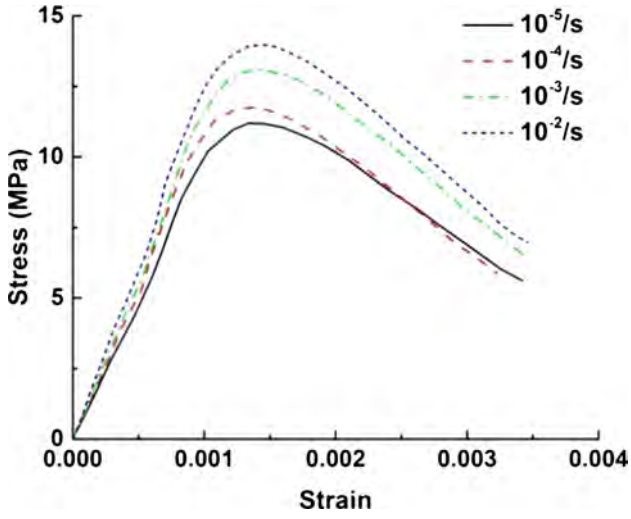

Fig. 2. Measured stress-strain curves of micro-concrete at different strain rates.

of strain rate, the values of ultimate compressive strength and Young's modulus become higher. Table 2 summarizes the calculated mean compressive strength and Young's modulus of the micro-concrete specimens. As compared with the quasi-static strain rate case (10^{-5} s^{-1}), the compressive strength increases by 5.4%, 17.2% and 24.7% at the strain rates of 10^{-4}, 10^{-3} and 10^{-2} s^{-1}, respectively. For each test specimen, the Young's modulus is measured in the stress range of 0 to 40% of the compressive strength. The mean values of the measured Young's modulus increase by 11.1%, 16.2% and 25.5% at the strain rates of 10^{-4}, 10^{-3} and 10^{-2} s^{-1} as compared with the quasi-static strain rate, respectively.

Table 2
Mean values of measured compressive strength and Young's modulus of the micro-concrete at different strain rates.

Strain rate (s^{-1})	Compressive strength (MPa)		Young's modulus (MPa)	
	Mean values	Difference	Mean values	Difference
10^{-5}	11.20	–	9484	–
10^{-4}	11.80	5.4%	10,538	11.1%
10^{-3}	13.13	17.2%	11,018	16.2%
10^{-2}	13.97	24.7%	11,898	25.5%

According to the regression analyses of the test results (as shown in Fig. 3), the DIFs for the compressive strength and Young's modulus of the micro-concrete can be obtained as

$$DIF_c = f_c^d / f_{cs} = 0.9892 + 0.08607 \lg(\dot{\varepsilon}_c / \dot{\varepsilon}_{cs}) \quad (1)$$

$$DIF_E = E_c^d / E_{cs} = 1.00974 + 0.08142 \lg(\dot{\varepsilon}_c / \dot{\varepsilon}_{cs}) \quad (2)$$

where f_c^d and E_c^d are the dynamic compressive strength and Young's modulus, respectively; f_{cs} and E_{cs} are the compressive strength and Young's modulus under quasi-static strain rate; $\dot{\varepsilon}_c$ is the strain rate of micro-concrete and $\dot{\varepsilon}_{cs} = 10^{-5}$ s^{-1} is the quasi-static strain rate.

As reviewed by Fu et al. [1], the influence of strain rate on the concrete compressive strain at maximum stress and at failure is a very controversial issue. Some researchers indicated that the concrete strain at failure slightly increased under dynamic loading rates (e.g. Watstein [26]; Scott et al. [27] and Mander et al. [28]). However, Dilger et al. [29] and Soroushian et al. [30] reported that the plastic strain of concrete actually decreased with the increase of loading rate. In addition, Mlakar et al. [31] concluded that the effect of loading rate on the concrete strain corresponding to the maximum stress can be neglected. According to the test results of micro-concrete of the present study, no obvious consistent increase or decrease in the concrete compressive strain at maximum stress and at failure was observed (as shown in Fig. 2). Therefore, the influence of loading rate on the concrete strain is not taken into account herein.

2.2. Iron wire

To investigate the dynamic tensile properties of iron wires under seismic loading rates, the iron wires with diameters of 1.6, 2.0 and 2.8 mm are tested using the MTS New 810 electro-hydraulic servo-controlled system (as shown in Fig. 4). In total four loading rates, namely 2.5×10^{-4}, 2.5×10^{-3}, 2.5×10^{-2} and $2.5 \times 10^{-1.4}$ s^{-1}, are taken into account. The loading rate of 2.5×10^{-4} corresponds to the quasi-static strain rate and the others are in the strain rate range of reinforcing steels induced by earthquakes. The loading scheme are almost the same with the dynamic compressive test of micro-concrete, i.e., at least three iron wire specimens are tested under each strain rate.

The averaged stress-strain curves of iron wires at various strain rates are calculated based on the test data, as depicted in Fig. 5. As

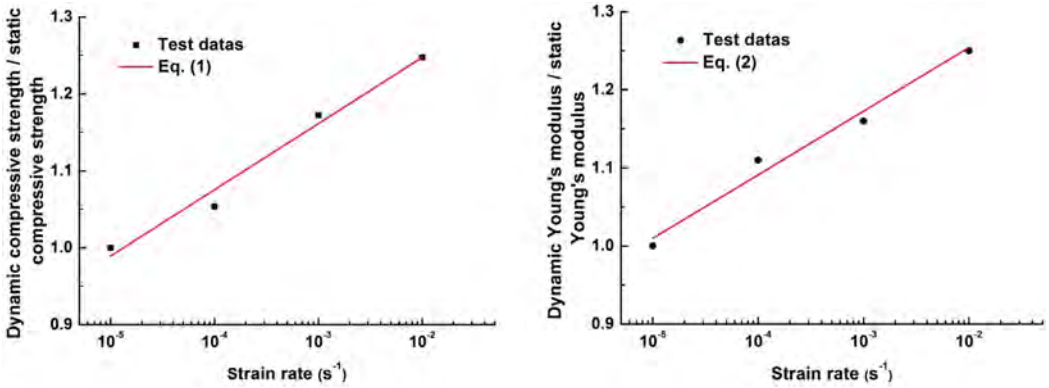

(a) Compressive strength (b) Young's modulus

Fig. 3. Mean values of the measured compressive strength and Young's modulus of micro-concrete at different strain rates.

(a) Test system and specimen setup (b) Failure of iron wires (D=2.0 mm)

Fig. 4. Dynamic test equipment and tensile failure mode of the iron wire specimens.

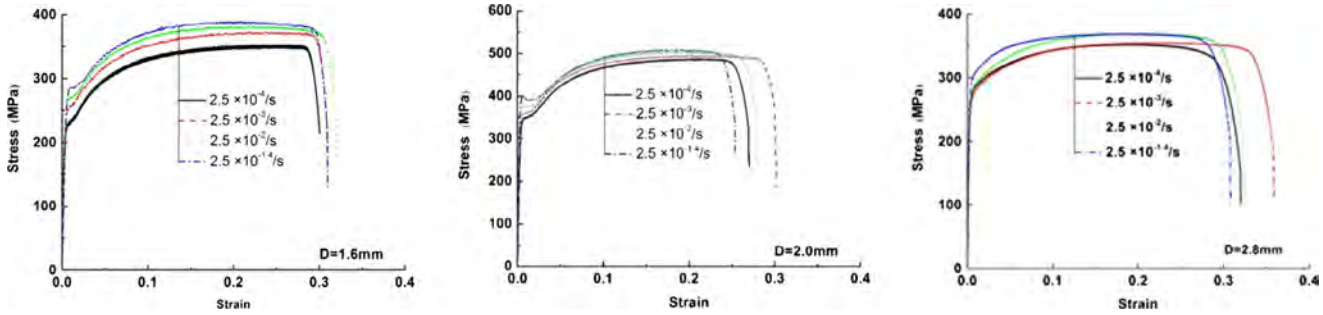

(a) D=1.6 mm (b) D=2.0 mm (c) D=2.8 mm

Fig. 5. Measured stress-strain curves of iron wire at different strain rates.

shown, the elastic moduli of the iron wires are basically the same under different strain rates. No obvious increase or decrease in yield strain and strain at maximum stress and at failure was observed. However, both of the tensile yield strength and ultimate strength increase with strain rate. The mean values of measured yield strength and ultimate tensile strength of iron wires with different diameters are summarized in Table 3. As compared with the quasi-static strain rate case ($2.5 \times 10^{-4}\ s^{-1}$), the yield strength at $2.5 \times 10^{-1.4}\ s^{-1}$ significantly increases by 20.69%, 12.11% and 9.14% for the iron wires with diameters of 1.6, 2.0 and 2.8 mm, respectively. The corresponding increasing degrees of the dynamic ultimate tensile strength are 8.72%, 5.99% and 3.15%, respectively.

According to the regression analyses of the test results (as depicted in Fig. 6), the DIFs for the yield strength and ultimate tensile strength of iron wire can be expressed by

$$DIF_y = f_{yd}/f_{ys} = 1.0 + 0.0456\lg(\dot{\varepsilon}_w/\dot{\varepsilon}_{w0}) \quad (3)$$

$$DIF_u = f_{ud}/f_{us} = 1.0 + 0.0212\lg(\dot{\varepsilon}_w/\dot{\varepsilon}_{w0}) \quad (4)$$

in which $\dot{\varepsilon}_w$ is the strain rate; $\dot{\varepsilon}_{w0}$ denotes the quasi-static strain rate; f_{ys} and f_{yd} are the quasi-static and dynamic yield strength, respectively; f_{us} and f_{ud} are the quasi-static and dynamic ultimate tensile strength, respectively.

Table 3
Measured yield strength and ultimate tensile strength of iron wires.

Diameter (mm)	Strain rate (s^{-1})	Yield strength (MPa)		Ultimate strength (MPa)	
		Mean values	Difference	Mean values	Difference
1.6	2.5×10^{-4}	238.55	–	356.34	–
	2.5×10^{-3}	251.39	5.38%	366.79	2.93%
	2.5×10^{-2}	264.40	10.84%	377.19	5.85%
	$2.5 \times 10^{-1.4}$	287.90	20.69%	387.42	8.72%
2	2.5×10^{-4}	354.67	–	486.35	–
	2.5×10^{-3}	361.64	1.97%	494.66	1.71%
	2.5×10^{-2}	375.78	5.95%	500.58	2.93%
	$2.5 \times 10^{-1.4}$	397.62	12.11%	515.47	5.99%
2.8	2.5×10^{-4}	273.54	–	352.52	–
	2.5×10^{-3}	279.41	2.15%	353.86	0.38%
	2.5×10^{-2}	285.80	4.48%	362.60	2.86%
	$2.5 \times 10^{-1.4}$	298.54	9.14%	363.63	3.15%

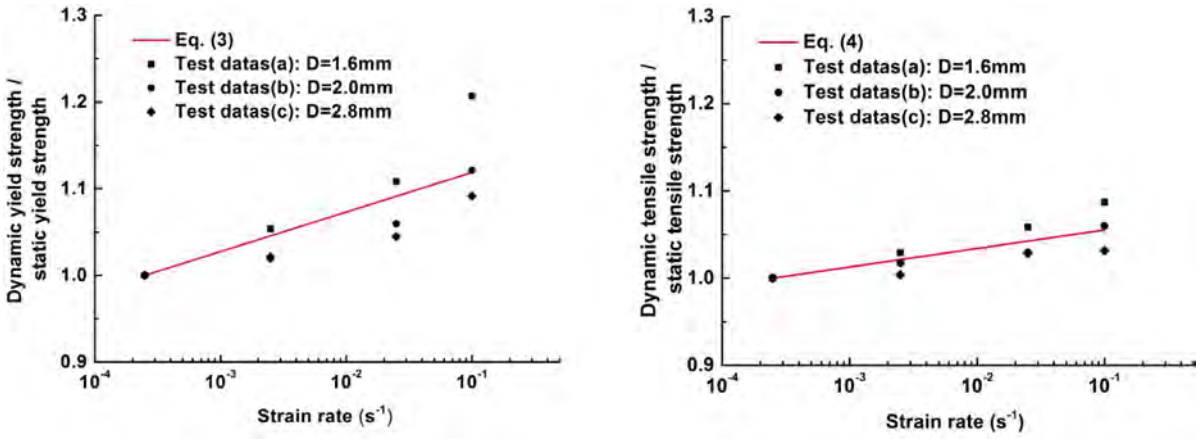

(a) Yield strength (b) Ultimate strength

Fig. 6. Tensile yield strength and ultimate strength of iron wires at different strain rates.

3. Shaking table test of RC structural model

The prototype building is a three-story asymmetric RC frame shear wall structure designed according to the Chinese Code for design of concrete structures [32]. The building has a plan dimension of 6 × 12 m^2 and a total height of 9.9 m with one bay and two spans. In a shaking table test, the dimensions of the structural model can inevitably affect the seismic responses of the structural model due to the size effect [33,34]. However, owing to the limitations of space and load capacity of shaking table equipment, it is very difficult to carry out a full-scale shaking table test of the prototype structure. Hence, the shaking table test of a 1/5 scaled RC structural model is carried out in this study to reproduce the structural seismic responses with inclusion of strain rate effect. By scaling down the geometric parameters and material properties of the prototype structure, the shaking table test specimen is designed and fabricated according to the similitude law [35,36]. The similitude scale factors of the specimen are summarized in Table 4.

The test specimen is casted by micro-concrete and iron wire, whose mechanical properties under dynamic loadings have been discussed in the previous section. Fig. 7 shows the configuration of the test specimen. The plan dimension, height and overall weight of the specimen are 1.2 × 2.4 m^2, 1.98 m and 1.7 t, respectively. The specimen is fixed on the shaking table, which has a plan dimension of 3 m × 4 m and a load carrying capacity of 10 t. As illustrated in Fig. 7(b), in total six accelerometers are placed on each floor to measure the acceleration time histories. To record the strains of concrete during the earthquake excitation, nine fiber

Table 4
Similitude relations for shaking table specimen.

Physical quantity	Similitude equation	Model/Prototype
Length	S_L	0.2
Young's modulus	S_E	0.25
Stress	$S_\sigma = S_E$	0.25
Strain	$S_\varepsilon = S_\sigma / S_E$	1
Density	$S_\rho = S_\sigma / (S_a \cdot S_L)$	1.25
Mass	$S_m = S_\rho \cdot S_L^3$	0.01
Stiffness	$S_K = S_E \cdot S_L$	0.05
Time	$S_T = (S_m / S_K)^{0.5}$	0.447
Frequency	$1/S_T$	2.237
Acceleration	S_a	1

Bragg grating (FBG) strain sensors are installed at the column and beam ends of the test specimen (Fig. 7(c)). The N-S and vertical components of the El Centro (EC) earthquake ground motion are selected as horizontal and vertical inputs in the shaking table test. The sequence of the input ground motions in the shaking table test is given in Table 5.

During the test process, the structural damage of the specimen after each loading stage is observed and recorded. After PGA = 0.24 g and PGA = 0.33 g, very minor cracks appear at the joints between the beams and side columns, these cracks initiate from the corners of columns and have a maximum width of 0.1 mm. With the increase of input ground motion intensity, the number of the cracks increases and the cracks become larger and deeper. After PGA = 0.5 g, the maximum crack width at the beam-column joints

(a) Shaking table specimen

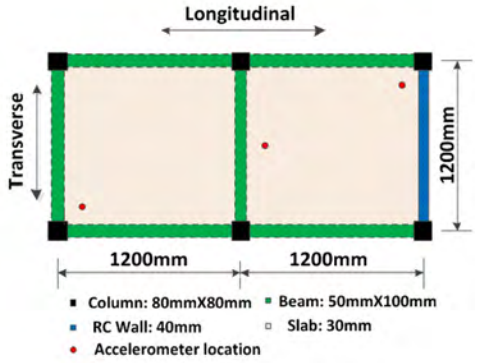

(b) Plan view

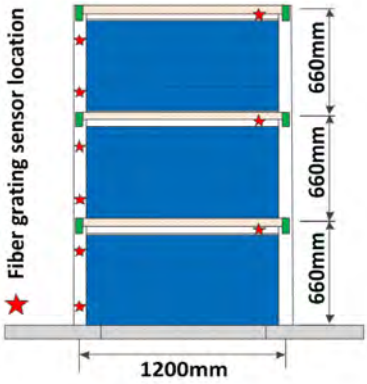

(c) Elevation-1 in transvers direction

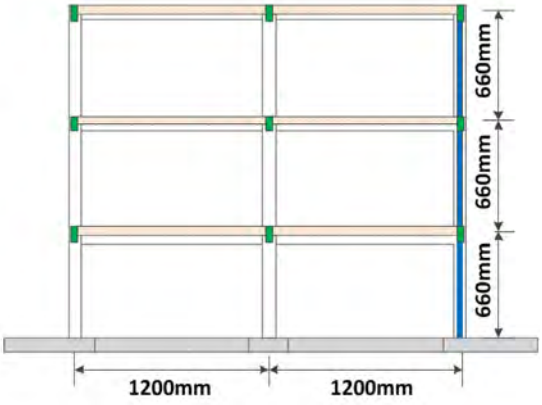

(d) Elevation-A in longitudinal direction

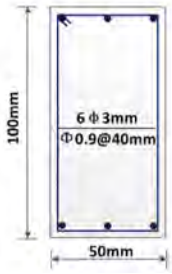

(e) Beam section

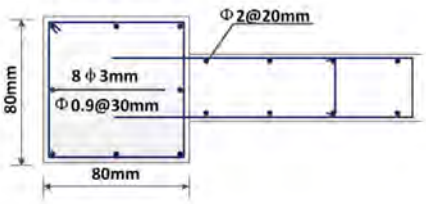

(f) Shear wall section

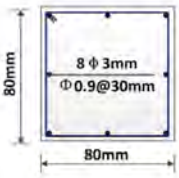

(g) Column section

Fig. 7. Configuration of the shaking table test specimen.

Table 5
Loading programme of the shaking table test.

Loading stages	PGA (g)	Direction
WN-1	0.005/–	Transverse/–
EC-1	0.16/0.04	Transverse/Vertical
EC-2	0.24/0.06	Transverse/Vertical
EC-3	0.33/0.09	Transverse/Vertical
EC-4	0.40/0.11	Transverse/Vertical
EC-5	0.50/0.15	Transverse/Vertical
EC-6	0.60/0.24	Transverse/Vertical
EC-7	0.70/0.40	Transverse/Vertical
EC-8	0.86/0.56	Transverse/Vertical

can reach 0.5 mm. The spalling of concrete cover is observed at the joints between beams and side columns after PGA = 0.6 g. When the PGA of the input motion increase to 0.86 g, the cracks at beams-column joints continue to develop and the widths of the existing cracks are significantly extended, some of the concrete cracks widened to over 1 mm. Moreover, the spalling of concrete becomes more serious than the previous loading stages. The local concrete crushing and reinforcement buckling at the beam-column joints between the second and third floor (after PGA = 0.86 g) are illustrated in Fig. 8.

Before each loading stage, the test specimen is excited under a random acceleration signal (i.e. white noise) of 0.005 g. The transfer function can be calculated by transforming the recorded acceleration responses into the frequency domain. The dynamic properties of the test specimen before each loading stage (i.e. the vibration frequencies and damping ratios) are estimated using the modal identification technique [34]. Fig. 9 shows the variations of the fundamental frequency and damping ratio of the structural model after different loading stages. It can be observed that the fundamental frequency of the specimen decreases and the damping ratio increases along with the test process owing to

(a) Joint-1 (b) Joint-2 (c) Joint-3

Fig. 8. Structural damage at the beam-column joints between the second and third floor (after PGA = 0.86 g).

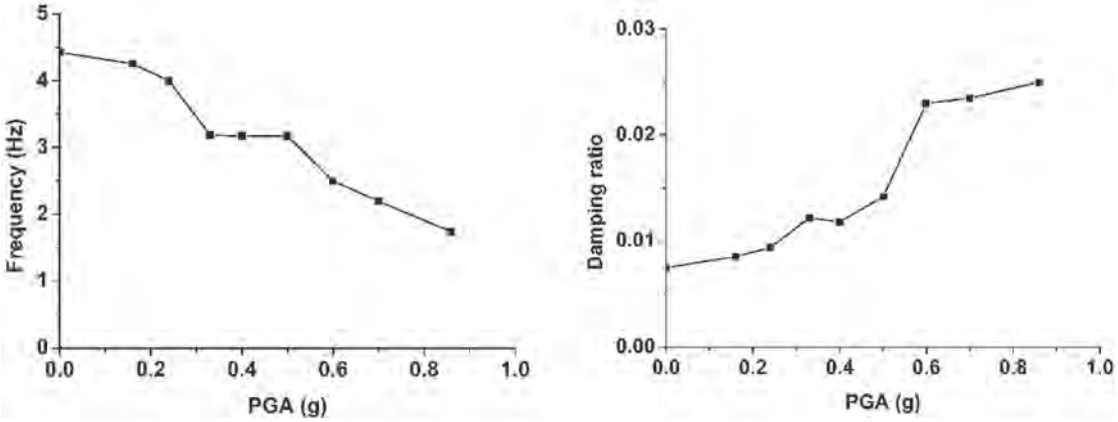

(a) Fundamental frequency (b) Damping ratio

Fig. 9. Variations of the structural fundamental frequency and damping ratio.

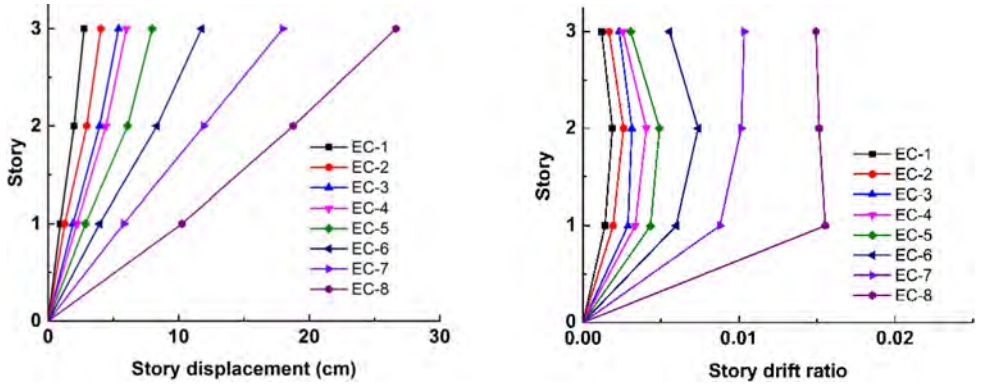

(a) Transverse story displacement (b) Transverse story drift ratios

Fig. 10. Maximum story displacement and story drift ratios of each floor under different input ground motion intensities.

the continuous accumulation of structural damage. By performing the baseline correction and filtering process for the recorded acceleration time histories of each floor, the displacement time histories are obtained using the double integral of acceleration in the time domain. The story displacement and drift ratios at each floor of the specimen under different input ground motion intensities are depicted in Fig. 10. It is shown that the structural responses significantly increase with the ground motion intensity, especially after PGA = 0.5 g. The evident increase of structural seismic demand at this PGA level results in a considerable damage of the shaking table specimen. As demonstrated in Fig. 9, both of the fundamental frequency and damping ratio of the specimen are substantially changed after PGA = 0.5 g.

The concrete strain rates of the structural members can be obtained by computing the derivatives of the concrete strains measured by the FBG strain sensors. The maximum concrete strain rates of the beams and columns at each floor are summarized in Table 6. It can be observed that the maximum strain rate of concrete increases with the increase of input ground motion intensity. The maximum concrete strain rates of the column members are 6.5×10^{-3}–6.8×10^{-2} s^{-1}, which are much higher than those of the beam members (2.0×10^{-3}–2.5×10^{-2} s^{-1}). Moreover, the strain rates of the first floor columns are higher than those of the second and third floor columns, while the strain rates of the first floor beams are basically lower than those of the beams in the upper floors.

Table 6
Recorded maximum concrete strain rates of column and beam members at different loading stages.

PGA (g)	Maximum strain rates of beams (s^{-1})			Maximum strain rates of columns (s^{-1})		
	1st floor	2nd floor	3rd floor	1st floor	2nd floor	3rd floor
0.16	2.0×10^{-3}	3.2×10^{-3}	3.5×10^{-3}	1.7×10^{-2}	6.9×10^{-3}	6.5×10^{-3}
0.24	2.2×10^{-3}	4.6×10^{-3}	4.8×10^{-3}	2.8×10^{-2}	1.1×10^{-2}	1.1×10^{-2}
0.33	2.3×10^{-3}	5.5×10^{-3}	6.5×10^{-3}	3.6×10^{-2}	1.0×10^{-2}	1.6×10^{-2}
0.40	2.8×10^{-3}	6.6×10^{-3}	6.8×10^{-3}	3.0×10^{-2}	1.2×10^{-2}	1.7×10^{-2}
0.50	3.7×10^{-3}	7.4×10^{-2}	6.8×10^{-3}	4.1×10^{-2}	1.2×10^{-2}	2.1×10^{-2}
0.60	6.1×10^{-3}	1.7×10^{-2}	8.2×10^{-3}	5.1×10^{-2}	1.2×10^{-2}	2.6×10^{-2}
0.70	9.6×10^{-3}	2.7×10^{-2}	1.0×10^{-2}	5.8×10^{-2}	1.5×10^{-2}	3.5×10^{-2}
0.86	9.0×10^{-3}	2.5×10^{-2}	1.9×10^{-2}	6.8×10^{-2}	1.5×10^{-2}	4.5×10^{-2}

4. Three-dimensional rate-dependent fiber beam-column element model

To perform rate-dependent seismic response analyses of RC structures, the ABAQUS platform is employed in this study. With an extensive library of material and element models, ABAQUS is widely used in the seismic analyses of engineering structural systems. However, owing to the lack of rate-dependent material models of concrete and reinforcing steel, the strain rate effect cannot be taken into account using the traditional beam elements in ABAQUS. To solve this problem, a novel three-dimensional fiber beam-column element model with the consideration of rate-dependent properties of RC materials is developed in this section.

4.1. Basic assumptions

The proposed beam-column element model is divided into longitudinal fibers [37,38], as shown in Fig. 11. The following basic assumptions are made to develop the rate-dependent fiber beam-column element: (1) The plane-section assumption is applicable during the element deformation history; (2) Neglecting the effects of cracking and bond slip; (3) The fiber constitutive models are one-dimensional stress-strain relations of RC materials; (4) Transverse shear behavior is linear elastic with a constant modulus and is independent with the axial deformation or transverse bending.

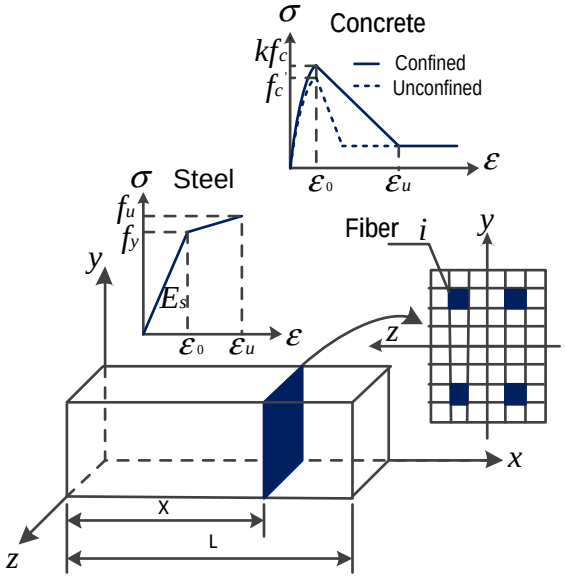

Fig. 11. Schematic view of the proposed fiber beam-column element.

4.2. Basic formulations of forces and deformations

The three-dimensional section forces of the fiber beam-column element include the axial force $N(x)$ and two bending moments $M_z(x)$ and $M_y(x)$. The corresponding section deformation vector can be represented by

$$\{d(x)\}^s = \phi_z(x)\ \phi_y(x)\ \varepsilon(x)^T \tag{5}$$

where $\varepsilon(x)$ denotes the axial strain along the longitudinal direction; $\phi_z(x)$ and $\phi_y(x)$ denote the two curvatures about the two orthogonal axes z and y, respectively.

The fiber strain at an arbitrary point (x,y,z) in the section is

$$\varepsilon(x,y,z) = [l(y,z)]\{d(x)\}^s \tag{6}$$

in which $[l(y,z)]$ is the section compatibility vector, which can be represented by $[l(y,z)] = [-y \quad z \quad 1]$.

The fiber stress of at point (x,y,z) in the section is calculated by

$$\sigma(x,y,z) = E_{\tan}(x,y,z)\varepsilon(x,y,z) \tag{7}$$

where the tangent modulus $E_{\tan}(x,y,z)$ and the stress $\sigma(x,y,z)$ can be determined by the stress-strain relation of the corresponding fiber. Based on the principle of virtual displacement, the section tangent stiffness matrix and the section resisting force can be computed by

$$[k(x)]^s = \int_A [l(y,z)]^T E_{\tan}(x,y,z)[l(y,z)]d_z d_y \tag{8}$$

$$\{F_R(x)\}^s = \int_A [l(y,z)^T \sigma(x,y,z)]d_z d_y \tag{9}$$

Using $n(x)$ to represent the number of fibers included in each section of the beam-column element. The fiber strains are assumed to be linearly distributed over the cross section. Thus, Eqs. (8) and (9) can be respectively reformulated as

$$[k(x)]^s = \begin{bmatrix} \sum_{i=1}^{n(x)} E_{i\tan}\cdot A_i \cdot y_i^2 & \sum_{i=1}^{n(x)} E_{i\tan}\cdot A_i \cdot y_i \cdot z_i & -\sum_{i=1}^{n(x)} E_{i\tan}\cdot A_i \cdot y_i \\ \sum_{i=1}^{n(x)} E_{i\tan}\cdot A_i \cdot y_i \cdot z_i & \sum_{i=1}^{n(x)} E_{i\tan}\cdot A_i \cdot z_i^2 & \sum_{i=1}^{n(x)} E_{i\tan}\cdot A_i \cdot z_i \\ -\sum_{i=1}^{n(x)} E_{i\tan}\cdot A_i \cdot y_i & \sum_{i=1}^{n(x)} E_{i\tan}\cdot A_i \cdot z_i & \sum_{i=1}^{n(x)} E_{i\tan}\cdot A_i \end{bmatrix} \tag{10}$$

$$\{F_R(x)\}^s = \begin{Bmatrix} -\sum_{i=1}^{n(x)} \sigma_i \cdot A_i \cdot y_i \\ \sum_{i=1}^{n(x)} \sigma_i \cdot A_i \cdot z_i \\ \sum_{i=1}^{n(x)} \sigma_i \cdot A_i \end{Bmatrix} \tag{11}$$

Finally, with the obtained section forces and deformations, the element forces and deformations can be calculated through the integration along the longitudinal axis (x-axis).

4.3. Constitutive models of fibers

4.3.1. Unconfined concrete stress-strain relation

For the concrete cover fibers, the monotonic envelope curves in tension and compression follows the stress-strain relation model specified in the Chinese code for design of concrete structures [32], as shown in Fig. 12. The stress-strain relations of concrete in tension is represented by

$$\sigma_t = (1 - d_t) E_c \varepsilon_t \tag{12}$$

$$d_t = \begin{cases} 1 - \rho_t(1.2 - 0.2x_t^5) & x_t \le 1 \\ 1 - \frac{\rho_t}{\alpha_t(x_t - 1)^{1.7} + x_t} & x_t > 1 \end{cases} \tag{13}$$

in which

$$\rho_t = \frac{f_{t,r}}{E_c \varepsilon_{t,r}} \tag{14}$$

$$x_t = \frac{\varepsilon}{\varepsilon_{t,r}} \tag{15}$$

where α_t is the parameter that representing the descending part of stress-strain curves in tension; $f_{t,r}$ is the uniaxial tensile strength; $\varepsilon_{t,r}$ is the tensile strain corresponding to $f_{t,r}$; and d_t is the damage parameter in tension.

The stress-strain relations of concrete in compression is written by

$$\sigma_c = (1 - d_c) E_c \varepsilon \tag{16}$$

$$d_c = \begin{cases} 1 - \frac{\rho_c n}{n - 1 + x_c^n} & x_c \le 1 \\ 1 - \frac{\rho_c}{\alpha_c(x_c - 1)^2 + x_c} & x_c > 1 \end{cases} \tag{17}$$

in which

$$n = \frac{E_c \varepsilon_{c,r}}{E_c \varepsilon_{c,r} - f_{c,r}} \tag{18}$$

$$x = \frac{\varepsilon}{\varepsilon_{c,r}} \tag{19}$$

$$\rho_c = \frac{f_{c,r}}{E_c \varepsilon_{c,r}} \tag{20}$$

where α_c is the parameter of the descending part of stress-strain curves in compression; $f_{c,r}$ is the uniaxial compressive strength; $\varepsilon_{c,r}$ is the compressive strain corresponding to $f_{c,r}$; and d_c is the damage parameter in compression.

4.3.2. Confined concrete stress-strain relation

To account for the confinement of stirrups, the modified Kent-Park model [39] is used to modify the peak stress, peak strain and the strain softening slope of the core concrete in compression. The stress-strain relation of the confined concrete (as shown in Fig. 13) is described as follows:

$$\sigma_c = \begin{cases} Kf_c' \left[2\left(\frac{\varepsilon_c}{\varepsilon_0}\right) - \left(\frac{\varepsilon_c}{\varepsilon_0}\right)^2 \right], & \varepsilon_c \le \varepsilon_0 \\ Kf_c'[1 - Z(\varepsilon_c - \varepsilon_0)] \ge 0.2Kf_c', & \varepsilon_0 \le \varepsilon_c \le \varepsilon_u \end{cases} \tag{21}$$

in which

$$\varepsilon_0 = 0.002K \tag{22}$$

$$K = 1 + \frac{\rho_s f_{yh}}{f_c'} \tag{23}$$

$$Z = \frac{0.5}{\frac{3 + 0.29 f_c'}{145 f_c' - 1000} + 0.75\rho_s \sqrt{\frac{h'}{s_h}} - 0.002K} \tag{24}$$

$$\varepsilon_u = 0.004 + 0.9\rho_s(f_{yh}/300) \tag{25}$$

where ε_0 is the peak strain of concrete in compression; ε_u is the strain corresponding to the stress of $0.2f_c$; K is the coefficient which account for the increasing compressive strength due to confinement of stirrups; Z defines the strain softening slope and depends on the coefficient K; f_c' is the cylinder compressive strength; f_{yh} is the yield strength of stirrups; ρ_s is the volume ratio of stirrups to the volume of concrete core; h' is the width of core concrete measured to the outside edge of stirrups; and s_h is the center spacing of stirrups.

4.3.3. Reinforcing steel stress-strain relation

The monotonic envelope curve of reinforcing steel presented by Esmaeily and Xiao [40] is employed in the simulation (as shown in Fig. 14(a)), the stress and strain relation of the reinforcement is expressed by

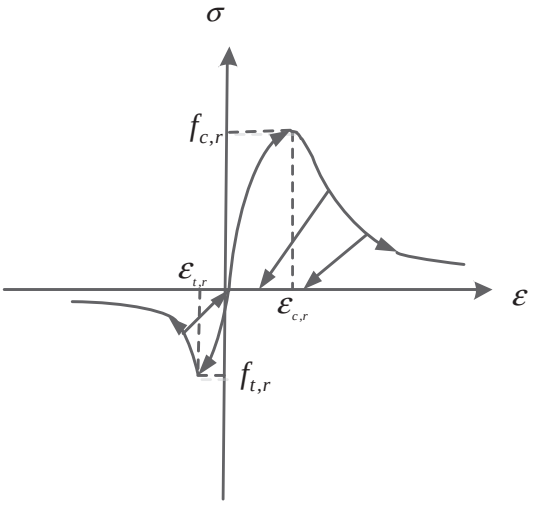

Fig. 12. The stress-strain relation of unconfined concrete.

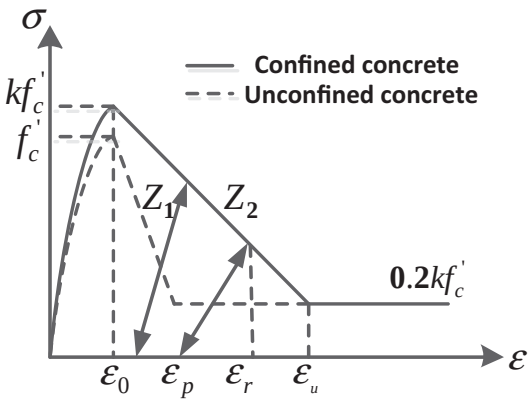

Fig. 13. The stress-strain relation of confined concrete.

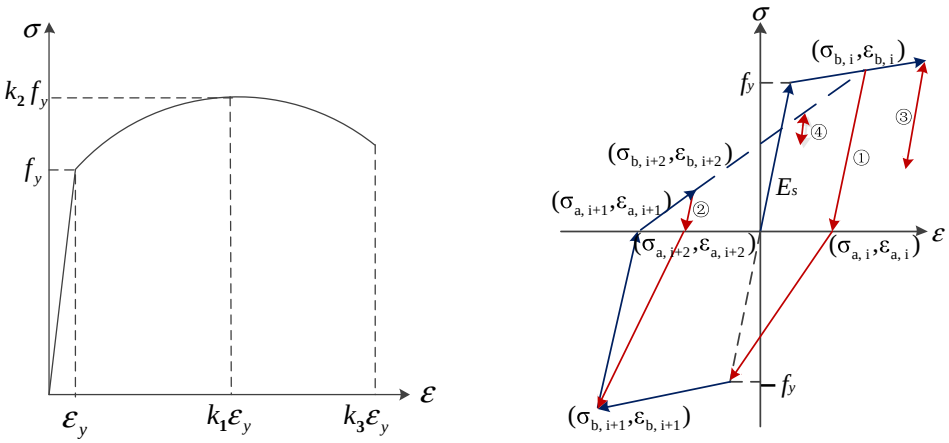

(a) Monotonic envelope curve (b) Cyclic constitutive relation

Fig. 14. The stress-strain relation of reinforcing steel.

$$\sigma = \begin{cases} E_s\varepsilon & \varepsilon \le \varepsilon_y \\ k_2 f_y - \frac{E_s(1-k_2)}{\varepsilon_y(k_1-1)^2}(\varepsilon - k_1\varepsilon_y)^2 & \varepsilon_y < \varepsilon < k_2\varepsilon_y \\ 0 & \varepsilon \ge k_3\varepsilon_y \end{cases} \quad (26)$$

where E_S is the Young's modulus of reinforcing steel; ε_y and f_y are respectively the strain and stress at the yielding point, respectively; ε_u is the strain at the ultimate stress; k_1 is the ratio of peak strain to yield strain; k_2 is the ratio of peak stress to yield stress and $k_3 = 40\varepsilon_y$.

The classical cyclic constitutive model of reinforcing steel described by Clough and Johnson [41] is simplified and modified to four branches, as shown in Fig. 14(b). It is noted that the last maximum strain is the point after which the response comes back to the bilinear envelope curve.

4.4. Consideration of the material rate-dependent properties

In this study, the above-mentioned constitutive models of concrete and reinforcing steel are incorporated in the ABAQUS platform through the user subroutine VUMAT [42]. It should be noted that the developed subroutine is not limited to specific stress-strain models of RC materials. The selected Ken-Park concrete model [39] and Esmaeily and Xiao [40] reinforcement model herein can be easily replaced by other available constitutive models of concrete and reinforcing steel. In the nonlinear seismic analyses of RC members or structures, the developed subroutine can be invoked in the explicit module of ABAQUS to update the material properties after each analysis step, in which the strain rate effect are taken into account using the DIFs of the key parameters of concrete and reinforcing steels. Thus, the influences of rate-dependent properties of RC materials on the dynamic responses of RC members or structures can be comprehensively taken into account.

To validate the reasonability and validity of the presented numerical model on the simulation of rate-dependent properties of RC materials, the FE models for the test specimens of micro-concrete and iron wire (D = 2 mm) in Section 2 are developed using the proposed beam-column element in ABAQUS. The DIFs of micro-concrete and iron wire estimated based on the test data are employed to represent the material dynamic properties in the beam-column models. Specifically, Eqs. (1) and (2) are used to calculate the DIFs for the compressive strength and Young's modulus of micro-concrete, while Eqs. (3) and (4) are applied to calculate the DIFs for the yield strength and ultimate tensile strength of iron wire.

The measured and simulated stress-strain curves of micro-concrete and iron wire at different strain rates are compared in Fig. 15(a) and (b). The dynamic material parameters of the micro-concrete and iron wire are respectively calculated based

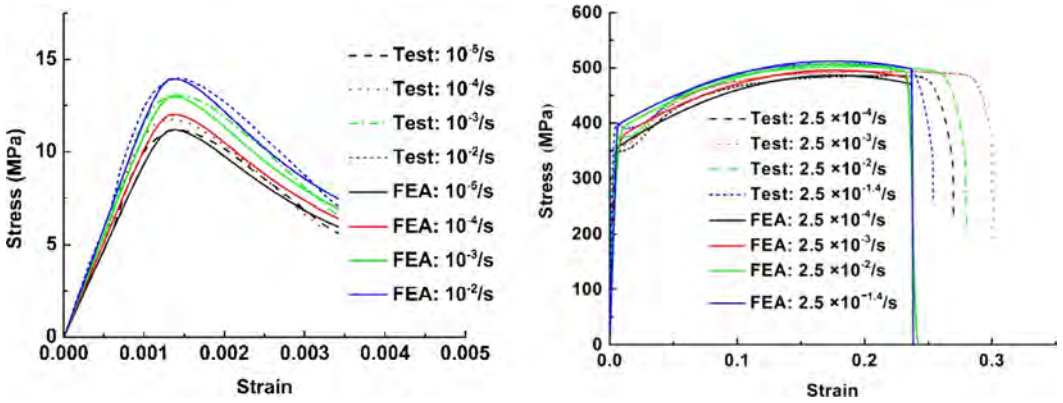

(a) Micro-concrete (b) Iron wire (D=2mm)

Fig. 15. Measured and simulated stress-strain curves of micro-concrete and iron wire at different strain rates.

Table 7
Key parameter values of micro-concrete and iron wire (D = 2 mm) obtained from experimental test and numerical simulation.

Micro-concrete	Compressive strength (MPa)			Young's modulus (MPa)		
Strain rate (s^{-1})	Measured	Simulated	Error	Measured	Simulated	Error
10^{-5}	11.20	11.18	0.18%	9484	9483	0.01%
10^{-4}	11.80	12.03	1.95%	10,538	10,266	2.65%
10^{-3}	13.13	12.99	1.08%	11,018	11,038	0.18%
10^{-2}	13.97	13.95	0.14%	11,898	11,811	0.74%
Iron wire	Yield strength (MPa)			Ultimate tensile strength (MPa)		
Strain rate (s^{-1})	Measured	Simulated	Error	Measured	Simulated	Error
2.5×10^{-4}	354.67	353.19	0.42%	486.35	486.36	–
2.5×10^{-3}	361.64	364.02	0.65%	494.66	496.88	0.45%
2.5×10^{-2}	375.78	371.68	1.10%	500.58	506.19	1.12%
$2.5 \times 10^{-1.4}$	397.62	397.41	0.05%	515.47	512.41	0.60%

on the test data and the numerical simulation results, as summarized in Table 7. It can be observed that the simulated stress-strain relations and parameter values of the micro-concrete and iron wire match well with the corresponding experimental data, indicating that the material rate-dependent properties can be precisely predicted using the proposed numerical model.

Fig. 16. Three-dimensional FE model of the shaking table specimen.

5. Numerical simulation of the shaking table test

5.1. FE modeling

To validate the applicability of the proposed numerical model on the simulation of seismic responses of RC structures with inclusion of stain rate effect, the three-dimensional FE model of the shaking table specimen is established using ABAQUS and the numerical results are compared with that of the experimental data obtained from the shaking table test. Fig. 16 illustrates the developed structural FE model, in which the RC beams and columns are simulated by the proposed dynamic fiber beam-column element and the RC walls and floors are simulated by the linear elastic shell element. It is noted that the damage of walls and floors of the shaking table specimen is very slight in the test process, even when the PGA of the input ground motion is scaled to 0.86 g. Therefore, the assumption of elastic walls and floors is reasonable. Moreover, the bottom nodes of the columns in the first floor are fixed on the ground and the rigid connections are used for the beam-column joints.

To consider the influence of rate-dependent properties of micro-concrete and iron wire, the developed subroutine is invoked in the numerical simulation to update the material parameters of the structural model. The constitutive model of the RC materials introduced in Section 4 and the DIFs of the micro-concrete and iron wire estimated in Section 2 are employed in the simulation. It should be noted that the DIF for the tensile strength of micro-concrete can also affect the structural seismic responses. However, it is unfortunate that no experimental data is available to evaluate the DIF for the tensile strength of micro-concrete in current literature. In this study, the DIF for the tensile strength of low-strength concrete presented by Lin et al. [43] is employed to approximately

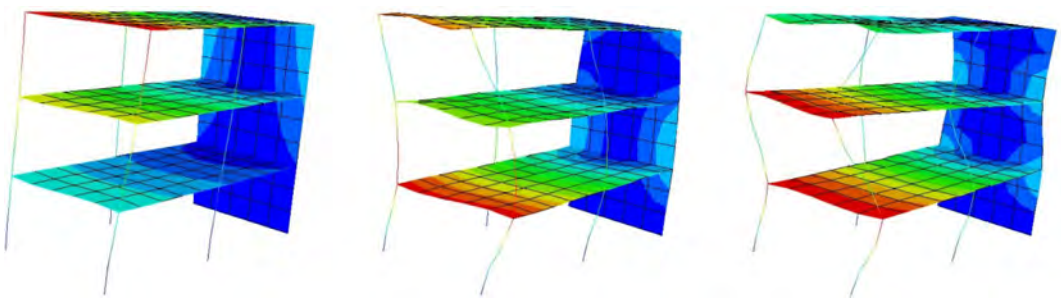

(a) 1st mode (f_1=4.41 Hz) (b) 2nd mode (f_2=14.13 Hz) (c) 3rd mode (f_3=24.41 Hz)

Fig. 17. The first three vibration modes of the FE model.

Table 8
Measured and simulated maximum roof displacements at different PGA levels.

PGA (g)	Test (cm)	Numerical simulation results			
		Rate-dependent (cm)	Error	Rate-independent (cm)	Error
0.16	0.273	0.259	−5.13%	0.295	8.06%
0.24	0.402	0.397	−1.24%	0.429	6.72%
0.33	0.536	0.552	2.99%	0.575	7.28%
0.40	0.596	0.671	2.58%	0.683	14.60%
0.50	0.793	0.749	−5.55%	0.855	7.82%
0.60	1.158	1.218	5.18%	1.319	13.90%
0.70	1.796	2.051	14.20%	2.077	15.65%
0.86	2.664	2.840	6.61%	2.869	7.70%

Table 9
Measured and simulated maximum story drift ratios at different PGA levels.

PGA (g)	Test (10^{-2})	Numerical simulation results			
		Rate-dependent (10^{-2})	Error	Rate-independent (10^{-2})	Error
0.16	0.188	0.188	–	0.188	–
0.24	0.259	0.258	−0.39%	0.267	3.09%
0.33	0.314	0.349	11.15%	0.362	15.29%
0.40	0.406	0.409	0.74%	0.439	8.13%
0.50	0.491	0.503	2.44%	0.529	7.74%
0.60	0.738	0.781	5.83%	0.812	10.03%
0.70	1.021	1.083	6.07%	1.178	15.38%
0.86	1.553	1.601	3.09%	1.771	14.04%

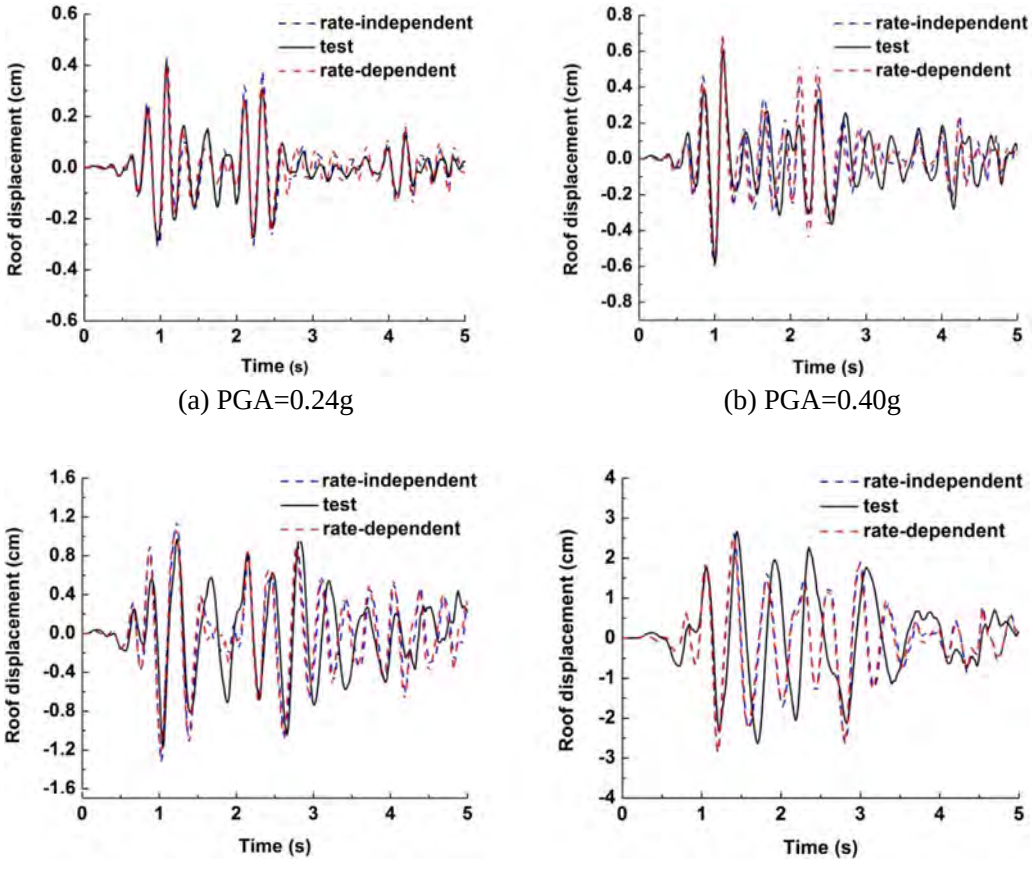

Fig. 18. Comparison between the roof displacement time histories obtained from the shaking table test and numerical simulations.

model the dynamic tensile strength of micro-concrete, which has the following form:

$$DIF_t = f_t^d / f_{ts} = 1.0 + 0.135 \lg(\dot{\varepsilon}_t / \dot{\varepsilon}_{ts}) \quad (27)$$

where f_t^d and f_{ts} are respectively the dynamic tensile strength and quasi-static tensile strength; $\dot{\varepsilon}_t$ is the strain rate; and $\dot{\varepsilon}_{ts}$ is the quasi-static strain rate, which is assumed to be $\dot{\varepsilon}_{ts} = 1 \times 10^{-5}$.

5.2. Numerical results

The modal analysis is firstly conducted in ABAQUS to assess the dynamic characteristic of the developed FE model. The first three vibration modes of the structural model are depicted in Fig. 17. The calculated fundamental frequency of the structural model is 4.41 Hz, which is very close to that measured for the shaking table specimen through white noise test (4.25 Hz). Hence, the dynamic characteristic of the FE model is in line with that of the test specimen.

Nonlinear time history analyses are performed to assess the effect of strain rate on the seismic response of the RC structure. Two numerical simulation cases are considered, namely the rate-dependent case using the proposed fiber beam-column element model with inclusion of strain rate effect, and the rate-independent case using the traditional ABAQUS fiber beam-column element (B31) without considering the rate-dependent properties of RC materials. The input ground motions employed in the numerical simulation are the same with those used in the shaking table test, i.e. the horizontal and vertical components of the El Centro (EC) earthquake motion. The numerically simulated and experimentally measured maximum roof displacements and story drift ratios at different PGA levels are summarized in Tables 8 and 9. The simulated roof displacement time histories and story drift ratios at 0.24 g, 0.4 g, 0.6 g and 0.86 g are compared with the corresponding test data in Figs. 18 and 19.

As shown in Tables 8 and 9, the maximum structural responses calculated by the proposed rate-dependent model match well with the experimental data of shaking table test. It is also shown in Figs. 18 and 19 that the numerically simulated time histories of roof displacements and story drift ratios are compatible with the corresponding test data at various PGA levels. Compared to the experimental data, the maximum response errors of the rate-dependent model are 14.20% for the peak roof displacement (PGA = 0.70 g) and 11.15% for the peak story drift ratio (PGA = 0.33 g), respectively. These errors are actually expected because it is very difficult to precisely control the material parameter uncertainties of micro-concrete and iron wire in manufacturing the shaking table specimen and the discrepancy between the specimen and the numerical model is inevitable. Moreover, neglecting the effects of concrete cracking and bond slip between reinforcements and concrete (as introduced in the assumptions of the proposed rate-dependent beam element model) may further influence the accuracy of the numerical simulation, especially when the specimen enters the nonlinear stage under high PGA levels.

It can also be seen from Tables 8 and 9 that the calculated structural seismic responses of the rate-dependent model are considerably lower as compared with those of the rate-independent model, and much closer to the experimental data obtained from the

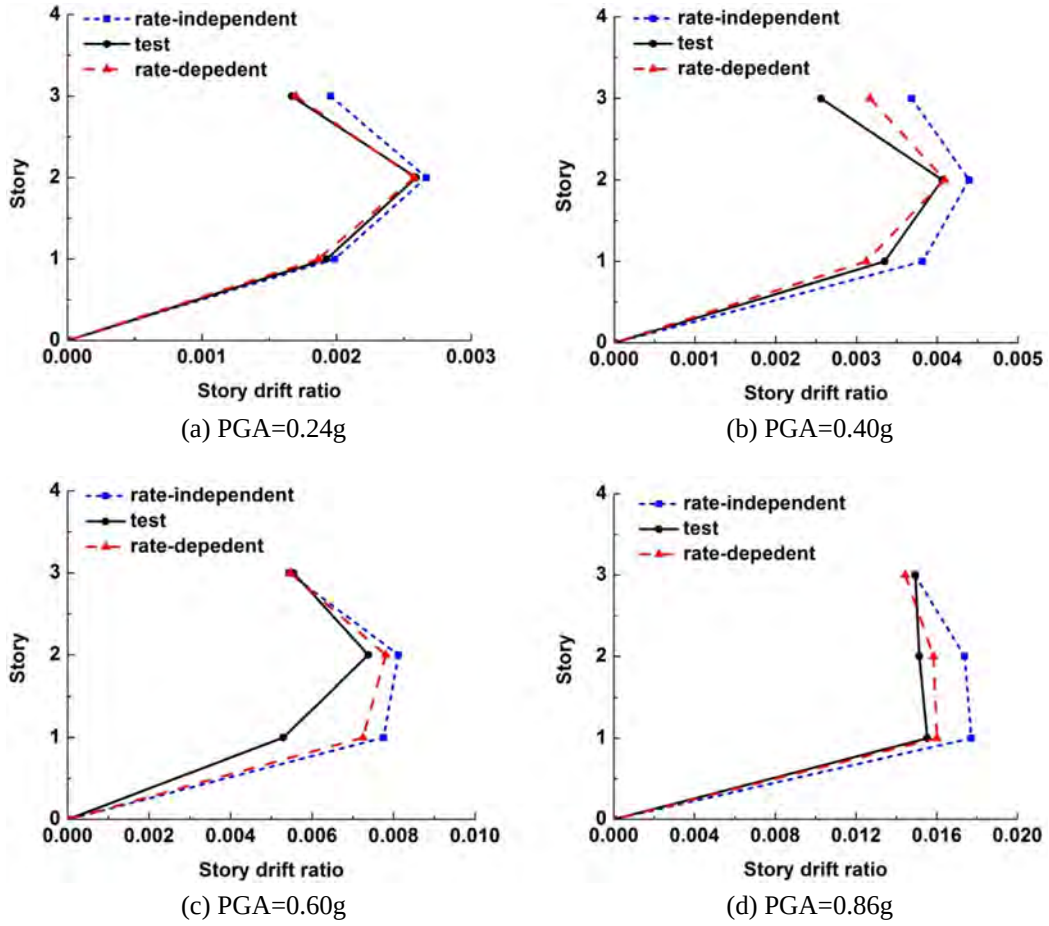

Fig. 19. Comparison between the maximum story drift ratios obtained from the shaking table test and numerical simulation.

shaking table test. Taking PGA = 0.6 g as an example, the rate-independent model overestimates the maximum roof displacement and story drift ratio by 13.90% and 10.03%, respectively; while the corresponding errors are reduced to 5.18% and 5.83% when using the rate-dependent model. This is owing to the fact that the effects of strain rates lead to higher strength of RC materials, which can enhance the structural resistant capacity and reduce the seismic responses. These simulation results demonstrate that the proposed rate-dependent fiber beam-column element model can reasonably capture the strain rate effect and provide more precise seismic response predictions of RC structures than the traditional beam-column element models.

6. Conclusions

In the present study, the influence of strain rate effect on the seismic responses of RC structures is comprehensively investigated through experimental tests and numerical simulations. The key findings are summarized as follows:

(1) The compressive strength and Young's modulus of the micro-concrete, as well as the yield strength and tensile ultimate strength of iron wire are all enhanced with the increasing loading rate. The DIFs for these key material parameters are estimated based on the experimental data of the dynamic loading tests.
(2) The strain rates of column and beam members in the shaking table specimen magnify with the input ground motion intensity. The peak strain rates of the columns are much higher than those of the beams. The effect of strain rate should not be neglected in the seismic response predictions of RC structures, especially under the excitations of strong earthquakes.
(3) It is validated by the shaking table test that the proposed rate-dependent fiber beam-column element model can more reasonably and accurately simulate the seismic responses of RC structures as compared with the traditional beam-column elements with static RC material constitutive models. The proposed numerical simulation method can yield precise seismic performance predictions of RC structures and provide beneficial recommendation and supplement for the seismic design codes of RC buildings.
(4) More investigations are needed to examine the effect of strain rate on the seismic responses of other types of RC structures, especially high-rise buildings. Moreover, the seismic vulnerability analyses of RC structures should be carried out in the future studies, in which the influence of rate-dependent properties of RC materials can be evaluated under a large number of input earthquake ground motions.

Conflict of interest

The authors declared that they have no conflicts of interest to the submitted work.

Acknowledgments

The authors would like to thank the financial supports from the National Key R&D Program of China (2016YFC0701108) and the State Key Program of National Natural Science Foundation of China (51738007) for carrying out this research. The supports from the Natural Science Foundation of Liaoning Province (20170540736) and the Program for Liaoning Excellent Talents in University (LJQ2015092) are also gratefully acknowledged.

References

[1] H.C. Fu, M.A. Erki, M. Seckin, Review of effects of loading rate on concrete in compression, J. Struct. Eng. 117 (12) (1991) 3645–3659.
[2] P.H. Bischoff, S.H. Perry, Compressive behaviour of concrete at high strain rates, Mater. Struct. 24 (6) (1991) 425–450.
[3] L.J. Malvar, C.A. Ross, Review of strain-rate effects for concrete in tension, ACI Mater. J. 95 (6) (1998) 735–739.
[4] R.J. Thomas, A.D. Sorensen, Review of strain rate effects for UHPC in tension, Constr. Build. Mater. 153 (2017) 846–856.
[5] P. Soroushian, K.B. Choi, Steel mechanical properties at different strain rates, J. Struct. Eng. 113 (4) (1987) 663–672.
[6] K.C. Chang, G.C. Lee, Strain rate effect on structural steel under cyclic loading, J. Eng. Mech. 113 (9) (1987) 1292–1301.
[7] J.I. Restrepo-Posada, L.L. Dodd, R. Park, N. Cooko, Variable affecting cyclic behavior of reinforcing steel, J. Struct. Eng. 120 (11) (1994) 3178–3196.
[8] L.J. Malvar, Review of static and dynamic properties of steel reinforcing bars, ACI Mater. J. 95 (5) (1998) 609–616.
[9] A. Filiatrault, M. Holleran, Stress-strain behavior of reinforcing steel and concrete under seismic strain rates and low temperatures, Mater. Struct. 34 (4) (2001) 235–239.
[10] E. Cadoni, L. Fenu, D. Forni, Strain rate behaviour in tension of austenitic stainless steel used for reinforcing bars, Constr. Build. Mater. 35 (2012) 399–407.
[11] M. Li, H.N. Li, Effects of strain rate on reinforced concrete structure under seismic loading, Adv. Struct. Eng. 15 (3) (2012) 461–475.
[12] J.L. Chen, J.W. Li, Z.X. Li, Experiment research on rate-dependent constitutive model of Q420 steel, Constr. Build. Mater. 153 (2017) 816–823.
[13] V.V. Bertero, D. Rea, S. Mahin, M.B. Atalay, Rate of loading effects on uncracked and repaired reinforced concrete members, in: Proceedings of 5th World Conference on Earthquake Engineering, Rome, Italy, 1973, pp. 1461–1470.
[14] S.M. Kulkarni, S.P. Shah, Response of reinforced concrete beams at high strain rates, ACI Struct. J. 95 (6) (1998) 705–715.
[15] S. Otani, T. Kaneko, H. Shiohara, Strain rate effect on performance of reinforced concrete members, in: Proceedings of FIB Symposium on Concrete Structures in Seismic Regions, Athens, Greece, 2003.
[16] H.N. Li, M. Li, Experimental and numerical study on dynamic properties of RC beam, Mag. Concrete Res. 65 (12) (2013) 744–756.
[17] W. Ghannoum, V. Saouma, G. Haussmann, Experimental investigations of loading rate effects in reinforced concrete columns, J. Struct. Eng. 138 (8) (2012) 1032–1041.
[18] D.B. Wang, H.N. Li, G. Li, Experimental tests on reinforced concrete columns under multi-dimensional dynamic loading, Constr. Build. Mater. 47 (5) (2013) 1167–1181.
[19] J. Carrillo, S.M. Alcocer, Experimental investigation on dynamic and quasi-static behaviour of low rise reinforced concrete walls, Earthq. Eng. Struct. D 42 (5) (2012) 635–652.
[20] A.K. Pandey, R. Kumar, D.K. Paul, D.N. Trikha, Strain rate model for dynamic analysis of reinforced concrete structures, J. Struct. Eng. 132 (9) (2006) 1391–1401.
[21] S. Guner, F.J. Vecchio, Simplified method for nonlinear dynamic analysis of shear-critical frames, ACI Mater. J. 109 (5) (2012) 727–737.
[22] C. Wang, J. Xiao, Z. Sun, Seismic analysis on recycled aggregate concrete frame considering strain rate effect, Int. J. Concr. Struct. Mater. 10 (3) (2016) 307–323.
[23] D. Asprone, R. Frascadore, M.D. Ludovico, A. Prota, G. Manfredi, Influence of strain rate on the seismic response of RC structures, Eng. Struct. 35 (2012) 29–36.
[24] Z. Yang, H.J. Liao, K.Y. Lou, Experimental study of the full curve of the stress-strain relationship for microconcrete, Eng. Mech. 19 (2) (2012) 90–94 (in Chinese).
[25] D.J. Shen, X.L. Lu, Experimental study on the mechanical property of microconcrete in model test, Civil Eng. J. 43 (10) (2010) 14–21 (in Chinese).
[26] D. Watstein, Effect of straining rate on the compressive strength and elastic properties of concrete, ACI J. 49 (1953) 729–744.
[27] B.D. Scott, R. Park, M.J.N. Priestley, Stress-strain behavior of concrete confined by overlapping hoops at low and high strain rates, ACI J. 79 (1) (1982) 13–27.
[28] J.B. Mander, M.J.N. Priestley, R. Park, Theoretical stress-strain model of confined concrete, J. Struct. Eng. 114 (8) (1988) 1804–1826.
[29] W.H. Dilger, R. Koch, R. Kowalczyk, Ductility of plain and confined concrete under different strain rates, ACI J. 81 (1) (1984) 73–81.
[30] P. Soroushian, K. Choi, A. Alhamad, Dynamic constitutive behavior of concrete, ACI J. 83 (2) (1986) 251–258.
[31] P.F. Mlakar, K.P. Vitaya-Udom, R.A. Cole, Dynamic tensile-compressive behavior of concrete, ACI J. 82 (4) (1985) 484–491.
[32] GB 50010-2010, Code for Design of Concrete Structures, China Architecture & Building Press, Beijing, 2010 (in Chinese).
[33] Z.P. Bazant, J. Planas, Fracture and Size Effect in Concrete and Other Quasibrittle Materials, CRC Press, 1997.
[34] X. Lu, Y. Chen, Y. Mao, Shaking table model test and numerical analysis of a supertall building with high-level transfer storey, Struct. Des. Tall Spec. 21 (10) (1985) 699–723.
[35] H.G. Harris, G.M. Sabnis, Structural Modeling and Experimental Techniques, CRC Press, Boca Raton, FL, 1999.

[36] X. Lu, G. Fu, W. Shi, W. Lu, Shake table model testing and its application, Struct. Des. Tall Spec. 17 (1) (2008) 181–201.
[37] F.F. Taucer, E. Spacone, F.C. Filippou, A Fiber Beam-column Element for Seismic Response Analysis of Reinforced Concrete Structures, EERC Report 91/17, Earthquake Engineering Research Center, University of California, Bekerley, CA, 1991.
[38] F.C. Filippou, D. Angelo, I. Ahmad, Nonlinear Static and Dynamic Analysis of Reinforced Concrete Subassemblages, EERC Report 92/08, Earthquake Engineering Research Center, University of California, Bekerley, CA, 1992.
[39] D.C. Kent, R. Park, Flexural members with confined concrete, J. Struct. Div. 97 (July) (1971) 1969–1990.
[40] F.C. Esmaeily, Y. Xiao, Behavior of reinforced concrete columns under variable axial loads: analysis, ACI Struct. J. 102 (5) (2005) 736–744.
[41] R.W. Clough, S.B. Johnson, Effect of stiffness degradation on earthquake ductility requirements, in: Proceedings of Japan Earthquake Engineering Symposium, Tokyo, Japan, 1966.
[42] K. Hibbitte, ABAQUS User Subroutines Reference Manual, HKS INC, 2005.
[43] G. Lin, D.M. Yan, Y. Yuan, Response of concrete to elevated-amplitude cyclic tension, ACI Mater. J. 104 (6) (2007) 561–566.